# Instability of Two-Dimensional Thermohaline Circulation

MICHAEL VELLINGA

*Institute for Marine and Atmospheric Research, Utrecht University, Utrecht, the Netherlands*

(Manuscript received 9 May 1995, in final form 26 July 1995)

ABSTRACT

Two different two-dimensional models of the thermohaline circulation of the ocean have been used to study the loss of stability of a thermally dominated symmetrical two-cell circulation. Although the models differ in their momentum budget, their behavior was qualitatively similar: the symmetrical solution was found to lose its stability at a critical strength of the salinity forcing with respect to two asymmetrical solutions that are mirror images of each other. The supercritical pitchfork bifurcation that describes this process was calculated with a numerical continuation technique. An analysis of the linear stability of the system yields an eigenfunction structure that allows the identification of the processes causing the instability. For the current surface forcing and parameter values that put the system in a thermal regime, this physical mechanism can be understood from meridional advection of salt and heat anomalies alone. This explains why the phenomenon of symmetry breaking is observed in such a wide range of studies and that model properties such as the choice of the convection scheme are only of quantitative importance.

## 1. Introduction

The thermohaline circulation (THC) of the ocean has been the subject of many studies the last few years. Different models, covering a great range of complexity, have been developed to study different aspects of this type of circulation. A good overview is provided by Weaver and Hughes (1992). Stommel (1961) discovered an important property of thermohaline flow: it can have multiple steady states. In his two-box model the existence of this multiplicity seems tied to a (nonlinear) meridional exchange of properties and dissimilar forcing of temperature and salinity: the restoring coefficients for temperature and salinity must be different. The model has no vertical structure, so vertical processes (like convection) are not a necessary ingredient to cause the multiplicity of steady states.

A situation for which vertical structure does seem to be crucial has been described by Welander (1986). He found that a two-box model, with one box mounted on top of the other (rather than next to the other), can exhibit self-sustained oscillations. The surface forcing is of mixed boundary conditions type: the temperature is restored and the salinity flux is specified. For a certain parameter setting, no steady state can be reached, and the system flip-flops between two states in which vertical mixing is dominated by either convection or diffusion. This periodic solution is absent in the Stommel (1961) model, and its existence seems related to the combined effects of mixed boundary conditions and convective mixing.

If it is true that these simple box models have identified the essential physical processes that lead to multiple equilibria and periodic solutions, these processes must also be present in more realistic models of the THC. Following the box models in complexity are two-dimensional, zonally averaged models. Indeed, the effect of an extra space dimension can be investigated as an intermediate stage, before considering the complete three-dimensional system. Several two-dimensional models have been described in the literature. All of these models have in common that the transport of heat and salt is governed by the two-dimensional advection–diffusion equations. The models differ, however, in the manner in which the momentum of the flow is calculated.

In their model, Marotzke et al. (1988) assume a balance between the meridional pressure gradient and vertical viscosity. In this model, it is indeed found that under mixed boundary conditions two different steady states are possible. These equilibria persist when the convective adjustment scheme is switched off. Besides creating regions with static instability, the major influence of this switching off is seen in the transitional behavior from an unstable to a stable equilibrium: the timescale of this transition is faster with convection present, and oscillatory behavior is reported, which seems to be absent in the case without convection. The existence of the asymmetric equilibria themselves is not affected. These results thus support the conclusions

*Corresponding author address:* Mr. Michael Vellinga, Institute for Marine & Atmospheric Research, Utrecht University, Princetonplein 5, 3584 CC Utrecht, the Netherlands.
E-mail: m.vellinga@fys.ruu.nl

that can be drawn from the experiments with box models with respect to instabilities of the thermohaline system.

A two-dimensional model that attempts to represent the effect of the rotation of the earth on the momentum balance has been formulated by Wright and Stocker (1991). The Coriolis force exerts a torque that must be parameterized in zonally averaged models. With a particular choice for this parameterization Wright and Stocker (1991) have carried out similar experiments as had been done by Marotzke et al. (1988), but now in a context more related to the oceanic situation. In general terms, the experiments of Wright and Stocker matched those of Marotzke et al. and show the instability of the symmetric state obtained under restoring boundary conditions, with respect to a change to mixed boundary conditions. Differences between the two models concern the spatial structure of the overturning cells and the internal timescales of transitions. The effect of a different momentum budget on the dynamical behavior seems not to be significant in the cases that have been reported.

This conclusion is confirmed by yet another two-dimensional model of the THC. Quon and Ghil (1992) have used the two-dimensional Navier–Stokes equations for the momentum budget, from which the Coriolis force is absent. This moves their model away from the oceanic situation. They report that, for a geometry with an aspect ratio of 0.1, at a certain strength of the salt flux the symmetrical two-cell solution becomes unstable with respect to an asymmetrical one-cell solution. By performing a series of time integrations they were able to construct the diagram of the associated pitchfork bifurcation. Thus again the same behavior is found (multiple equilibria under mixed boundary conditions).

So, experiments with different models suggest that the loss of symmetry under mixed boundary conditions is a generic property of thermohaline flow. It is desirable to assess how sensitive this process is for details of the momentum budget and, if this sensitivity is small, why this should be so. For that purpose we have subjected two models to the same experiment: the model formulated by Quon and Ghil (1992) and the one by Wright and Stocker (1992). Both models were forced by mixed surface boundary conditions, and the strength of the salinity flux was varied.

Most large-scale ocean models apply a small aspect ratio and hydrostatic approximation. In such models, a parameterization must be implemented to mimic the effect of nonresolved convective processes. To examine the influence of this parameterization on the process of symmetry breaking, both models were modified on that point. In their original formulation the models are either nonhydrostatic (Quon and Ghil) or use the "complete mixing scheme" (Wright and Stocker). In the present study, an implicit vertical diffusion scheme (Marotzke 1991) has been included in the transport equations for heat and salt of both models. This choice enables us to compare different parameterization schemes (Wright and Stocker) and hydrostatic versus nonhydrostatic effects (Quon and Ghil).

To perform such model analyses by time integration is very time consuming. Moreover, unstable solutions that connect branches of stable solutions cannot be found in this way and must be guessed at. Therefore, in this study a numerical continuation technique is used with which one can calculate a branch of both stable and unstable equilibrium solutions in parameter space. We will construct bifurcation diagrams that give the desired systematic answers to the following questions: how many solutions exist for a certain parameter setting, how are the solutions connected, what are their stability properties and how do these change when a model parameter is varied? This approach has already been used to study low-dimensional systems, for example, box-models like the one for the ocean–atmosphere circulation by Wang and Birchfield (1992), as well as more complicated systems like that of the wind-driven circulation; see Speich et al. (1996). Only stationary and periodic solutions can be determined with this technique, the transient solutions cannot.

The models are described in sections 2 and 3, the numerical solution technique is described in section 4, the experiments are shown in section 5, and an analysis of the linear stability of the models is presented in section 6. Conclusions and a discussion follow in section 7.

## 2. The hydrostatic Navier–Stokes model

### *a. Equations and scaling*

The model formulated in this section is based on the Navier–Stokes (NS) equations simplified by the Boussinesq approximation, the continuity equation, the transport equations for heat and salt, and a linear equation of state, all formulated on a nonrotating two-dimensional Cartesian frame. These equations also form the basis of the model of Quon and Ghil (1992). However, there is an essential difference between their model and the current one: the present model will exploit the smallness of the aspect ratio $\delta$ that is so characteristic for large-scale oceanic flow, typically $O(10^{-3})$. This observation motivates why as a zeroth-order approximation vertical accelerations that are of $O(\delta)$ can be neglected; that is, the hydrostatic approximation will be applied to the vertical momentum equation. Quon and Ghil generally used an aspect ratio of 0.1 in their nonhydrostatic model. The model variables are velocity $v$, $w$, temperature $T$, salinity $S$, density $\rho$ (constant reference density $\rho_0$), and pressure $\tilde{p}$ (where the total pressure $p$ is written as $p = \tilde{p} - \rho_0 gz$). By scale analysis it can be shown that for circulations on a large spatial and temporal scale local accelerations are negligible. The steady-state momentum equations

are used; that is, the velocity field follows diagnostically from the temperature and salinity fields. This step does not affect the equilibrium solutions, and it is assumed that even for unstable modes local accelerations are unimportant:

$$v\frac{\partial v}{\partial y} + w\frac{\partial v}{\partial z} = -\frac{1}{\rho_0}\frac{\partial \tilde{p}}{\partial y} + A_h\frac{\partial^2 v}{\partial y^2} + A_v\frac{\partial^2 v}{\partial z^2} \quad (1)$$

$$v\frac{\partial w}{\partial y} + w\frac{\partial w}{\partial z} = -\frac{1}{\rho_0}\frac{\partial \tilde{p}}{\partial z} - \left(\frac{\rho - \rho_0}{\rho_0}\right)g + A_h\frac{\partial^2 w}{\partial y^2} + A_v\frac{\partial^2 w}{\partial z^2} \quad (2)$$

$$\frac{\partial v}{\partial y} + \frac{\partial w}{\partial z} = 0 \quad (3)$$

$$\frac{\partial (S,T)}{\partial t} + v\frac{\partial (S,T)}{\partial y} + w\frac{\partial (S,T)}{\partial z} = \frac{\partial}{\partial y}\left(\kappa_h\frac{\partial (S,T)}{\partial y}\right) + \frac{\partial}{\partial z}\left(\kappa_v\frac{\partial (S,T)}{\partial z}\right) \quad (4)$$

$$\rho = \rho_0(1 - \alpha(T - T_0) + \beta(S - S_0)). \quad (5)$$

We define $\sigma \equiv (\rho - \rho_0)/\rho_0$ and introduce the following scaling to find the nondimensional equations (primes denote dimensionless variables): $t = L/Vt'$; $(v, w) = (V, VD/L)(v', w')$; $(y, z) = (L, D)(y', z')$; $S - S_0 = \bar{S}S'$; $T - T_0 = \bar{T}T'$; $\sigma = \alpha\bar{T}\sigma'$; $\tilde{p} = gD\rho_0\alpha\bar{T}p'$.

With a combined viscous–diffusive velocity scale $V = (\kappa_h A_h)^{1/2}/L$ we apply this scaling to (1)–(5) to get (omitting primes)

$$v\frac{\partial v}{\partial y} + w\frac{\partial v}{\partial z} = -\mathrm{Ra}\frac{\partial p}{\partial y} + \mathrm{Pr}^{-1/2}\frac{\partial^2 v}{\partial y^2} + r_v\,\mathrm{Pr}^{-1/2}\frac{\partial^2 v}{\partial z^2} \quad (6)$$

$$\delta\left(v\frac{\partial w}{\partial y} + w\frac{\partial w}{\partial z}\right) = -\mathrm{Ra}\delta^{-1}\left(\frac{\partial p}{\partial z} + \sigma\right) + \delta\mathrm{Pr}^{-1/2}\frac{\partial^2 w}{\partial y^2} + \delta r_v\mathrm{Pr}^{-1/2}\frac{\partial^2 w}{\partial z^2} \quad (7)$$

$$\frac{\partial v}{\partial y} + \frac{\partial w}{\partial z} = 0 \quad (8)$$

$$\frac{\partial (S,T)}{\partial t} + v\frac{\partial (S,T)}{\partial y} + w\frac{\partial (S,T)}{\partial z} = \frac{\partial}{\partial y}\left(\mathrm{Pr}^{1/2}\frac{\partial (S,T)}{\partial y}\right) + \frac{\partial}{\partial z}\left(r_d\mathrm{Pr}^{1/2}\frac{\partial (S,T)}{\partial z}\right) \quad (9)$$

$$\sigma = -T + R_S S. \quad (10)$$

As can be seen from the equation of state, $S$ and $T$ now indicate fluctuations in the temperature and salinity fields—that is, departures from the basic states, $S_0$, and $T_0$. The transport equations depend only on the gradients of $S$ and $T$ and are not affected by this re-definition. In the above, the following dimensionless parameters have been introduced:

$\delta = D/L$: aspect ratio
$\mathrm{Ra} = gD\alpha\bar{T}L^2/(\kappa_h A_h)$: Rayleigh number
$\mathrm{Pr} = \kappa_h/A_h$: Prandtl number
$R_S = \beta\bar{S}/(\alpha\bar{T})$: buoyancy ratio.

The factors that multiply the Prandtl number are

$$r_v = \frac{A_v}{\delta^2 A_h}; \quad r_d = \frac{\kappa_v}{\delta^2\kappa_h}.$$

With typical values for the horizontal turbulent mixing coefficients of $10^3$ m$^2$ s$^{-1}$, $10^{-3}$ m$^2$ s$^{-1}$ for the vertical mixing coefficients, and a typical aspect ratio for the large-scale circulation of $10^{-3}$ we see that $r_v = r_d = O(1)$. In (7) we take the limit $\delta \to 0$, while $\mathrm{Pr}^{1/2}$ is assumed to be $O(\delta)$ or bigger. The vertical momentum equation thus simplifies (to zeroth order in $\delta$) to the hydrostatic balance:

$$\frac{\partial p}{\partial z} = -\sigma. \quad (11)$$

Finally, the number of unknowns can be reduced by one if the pressure is eliminated. If (6) is differentiated with respect to $z$ and the hydrostatic equation (11) is differentiated with respect to $y$, the two can be combined to give

$$\frac{\partial}{\partial z}\left(v\frac{\partial v}{\partial y} + w\frac{\partial v}{\partial z}\right) = \mathrm{Ra}\frac{\partial \sigma}{\partial y} + \frac{\partial}{\partial z}\left(\mathrm{Pr}^{-1/2}\frac{\partial^2 v}{\partial y^2} + r_v\,\mathrm{Pr}^{-1/2}\frac{\partial^2 v}{\partial z^2}\right). \quad (12)$$

Solving (12) gives the baroclinic part of the flow. An additional condition is needed to determine the barotropic component, and thereby the complete flow. Conservation of mass gives this extra condition: for any latitude $y$, the surface integral of the continuity equation over the area defined by $[y, L] \times [0, D]$ is expressed as a contour integral (using Green's theorem). It states that if no water is entering or leaving the basin, there can be no net northward mass flux:

$$\int_0^1 v(y, z)dz = 0. \quad (13)$$

Equations (12) and (13) together fully determine the flow field and form, together with (8), (9), and (10), the NS model.

*b. Boundary conditions*

The equations are solved on a rectangular geometry with insulating vertical walls at $y = \pm 1$, a flat bottom at $z = 0$, and the sea surface at $z = 1$. The boundary conditions that go with the equations of the hydrostatic NS model are the following (in dimensionless form, $n$ defines the normal direction):

$$v = w = 0 \quad \text{at} \quad z = 0 \tag{14}$$

$$\frac{\partial v}{\partial z} = 0; \quad w = 0 \quad \text{at} \quad z = 1 \tag{15}$$

$$v = \frac{\partial w}{\partial y} = 0 \quad \text{at} \quad y = \pm 1 \tag{16}$$

$$\frac{\partial T}{\partial n} = \frac{\partial S}{\partial n} = 0 \quad \text{at} \quad z = 0, \quad y = \pm 1 \tag{17}$$

$$-\frac{\partial S}{\partial z} = \mu_s'(S - S^*(y)) + \hat{Q}_s Q_s^*(y) \quad \text{at} \quad z = 1 \tag{18}$$

$$-\frac{\partial T}{\partial z} = \mu_h'(T - T^*(y)) + \hat{Q}_h Q_h^*(y) \quad \text{at} \quad z = 1, \tag{19}$$

where $S^*(y)$ and $Q_s^*(y)$ are $O(1)$ shape functions of the restoring salinity field and the salinity flux, respectively. The same applies to the shape functions in the boundary condition for the surface temperature. $\hat{Q}_s = Q_{s,0}D/(A_v\bar{S})$ is the scaled amplitude of the salt flux, similarly for the heat flux. The nondimensional restoring coefficient $\mu_s'$ follows from its dimensional counterpart $\mu_s$: $\mu_s' = \mu_s D/A_v$, similarly for $\mu_h'$. In the formulation of the surface flux of salt and heat, the restoring coefficient $\mu_{s,h}'$ and flux strength $\hat{Q}_{s,t}$ allow the use of restoring ($\mu' \neq 0$, $\hat{Q} = 0$) or flux boundary conditions ($\mu' = 0$, $\hat{Q} \neq 0$). Mixed boundary conditions result if $\mu_s' = 0$, $\hat{Q}_s \neq 0$, $\mu_h'$ is "large," and $Q_h = 0$.

If the system is forced at the surface by a flux condition on, say, salinity, the salinity field is determined up to an additive constant. This is so because the model does not depend on the density and salinity itself but only on the respective gradients. One method of obtaining a unique solution would be to impose a global salinity constraint. Since this involves a global integral of the salinity field, which is very unattractive from a computational point of view, we do not use this method. Instead, out of the whole family of solutions that satisfy the model equations one is selected where the salinity in a certain point has a fixed value. Lest we introduce any artificial asymmetry in the system, the centermost point of the basin is chosen for this. If the solution were calculated by means of time integration, the initial condition would determine this salinity value.

*c. Convection scheme*

The hydrostatic approximation eliminates vertical accelerations from the model. An implicit vertical diffusion scheme (IVD) has been used as a parameterization for convective processes. It is assumed that convective mixing causes a vertical homogenization of the salinity and temperature fields in those areas where stratification would be gravitationally unstable. In the IVD parameterization this is achieved by letting the strength of vertical diffusion of heat and salt strongly increase if the vertical density gradient becomes positive (e.g., see Marotzke 1991). In view of the numerical continuation method that will be used, this dependence of the diffusion coefficient on density, although strong, needs to be continuous. This can be realized if the strength of convective mixing is modeled via a hyperbolic tangent. That is, we write in (9)

$$r_d \,\mathrm{Pr}^{1/2} \Rightarrow r_d \mathrm{Pr}^{1/2}[1 + F(\partial\sigma/\partial z)] \tag{20}$$

with

$$F(\partial\sigma/\partial z) \equiv F_0/2\left(1 + \tanh\left[\frac{1}{a}\frac{\partial\sigma}{\partial z}\right]\right).$$

The strength of the convective mixing is measured by the coefficient $F_0$. The slope of the shape function $F$ at neutral stability ($\partial\sigma/\partial z = 0$) is $1/a$, thus indicating that the smaller $a$ is, the steeper the jump that separates situations with and without convective activity. Due to the finite value of $a$, convective adjustment near neutral stability ($\partial\sigma/\partial z = 0$) is not "perfect": weak instabilities may survive and subcritical mixing for weakly stable stratifications occurs. Extremely steep jumps for very small $a$ greatly increase the numerical burden of calculating solutions. In the experiments $a = 0.1$ and $F_0 = 6$ is used.

## 3. The Wright and Stocker model

*a. Equations*

The equations that form the starting point of the Wright and Stocker (1992, hereafter WS) model are the zonally averaged geostrophic equations, the hydrostatic equation, the continuity equation, the transport equations for heat and salt, and the equation of state. For the scaling of all but the first two equations, the reader is referred to section (2a) on the hydrostatic NS model—the two models do not differ in that respect. The WS model is formulated on a spherical coordinate frame $(\lambda, \theta, z)$. For the sake of brevity, the formulation of the continuity equation and transport equations for heat and salt on the spherical frame is omitted. It can be found in Pedlosky (1987). The (dimensional) momentum equations of the WS model are

$$-2\Omega v \sin\theta = -\frac{1}{\rho_0}\frac{1}{r_0\cos\theta}\frac{\Delta P}{\Delta\Lambda} \tag{21}$$

$$\frac{1}{\rho_0}\frac{\partial p}{\partial z} = -\sigma g. \tag{22}$$

The notation is conventional; $\Delta P$ is the east–west pressure difference, and $\Delta\Lambda$ the zonal width of the basin (assumed constant). Equation (21) is differentiated with respect to $z$, while the hydrostatic approximation is applied to the east–west pressure difference. Combining the results gives a thermal wind equation:

$$-2\Omega \sin\theta \frac{\partial v}{\partial z} = \frac{g}{r_0 \Delta\Lambda} \frac{1}{\cos\theta} \Delta\sigma.$$

This equation is now scaled with the same scaling quantities as the NS model, in section 2a, with the only difference that for the horizontal length scale $L$ the radius of the earth $r_0$ is chosen

$$-\sin\theta \frac{\partial v}{\partial z} = \frac{gD\alpha\bar{T}}{2\Omega V r_0 \Delta\Lambda} \frac{1}{\cos\theta} \Delta\sigma. \tag{23}$$

Wright and Stocker (1992) postulate that the east–west density difference $\Delta\sigma$ can be expressed in terms of the north–south density gradient (dimensional as well as nondimensional):

$$\Delta\sigma = -\epsilon_0 \Delta\Lambda \sin 2\theta \frac{\partial \sigma}{\partial \theta}. \tag{24}$$

From comparison with GCM results, typically the tuning parameter $\epsilon_0$ is $O(0.1)$. The usefulness of this parameterization has been shown in different applications, for example, Wright and Stocker (1992), Stocker et al. (1992), Harvey (1992), and Hovine and Fichefet (1994). In a more rigorous analysis based on vorticity dynamics Wright et al. (1995) have demonstrated that a relation between the east–west density difference and the zonally averaged density exists, though generally a more complicated one than that of (24). If (24) is inserted into the thermal wind equation (23), one finds the relation between the meridional velocity and the density field that replaces (12):

$$\frac{\partial v}{\partial z} = 2\epsilon_0 \mathrm{Pr}^{1/2} E \,\mathrm{Ra} \frac{\partial \sigma}{\partial \theta} \equiv B \frac{\partial \sigma}{\partial \theta}, \tag{25}$$

$E$ is the Ekman number: $E = A_h/(2\Omega r_0^2)$. The parameter $B$ controls the strength of the forcing of the velocity by the density field.

### b. Boundary conditions

The boundary conditions on the temperature and salinity field are identical to those for the hydrostatic NS model and can be found in section 2b. The equation for $v$ (25) is first order in $z$. So, formally, only one condition in the $z$ direction can be imposed. As in section 2b, an integral form of the continuity equation provides this condition:

$$\int_0^1 v(\theta, z) \cos\theta dz = 0. \tag{26}$$

Equation (25) for $v$ does not allow other boundary conditions, such as one of no-normal flow at meridional walls. At those points we demand that $v$ be zero, a condition to which the solution adapts through a boundary layer that falls within the grid resolution and that is not explicitly resolved. For the velocity field, we then have the following set of boundary conditions:

$$v = 0 \quad \text{at} \quad \theta = \pm\theta_{\max}$$

$$w = 0 \quad \text{at} \quad z = 0 \quad \text{and at} \quad z = 1.$$

Bottom stress (friction) and surface stress (wind forcing) are neglected here. The latter could be included either by imposing a vertical Ekman velocity at the surface of the model (then representing the base of the Ekman layer) or by distributing this stress over the top (Ekman) layer of the model as a body force, like in Wright and Stocker (1992).

## 4. Numerical solution procedure

The partial differential equations (8), (9), (12), and (25) are discretized in space on an Arakawa C-grid (see Arakawa and Lamb 1977), which ensures conservation of mass, salt, and heat. Central differences have been used to calculate fluxes across cell boundaries. An equidistant Cartesian grid was used in the experiments with the NS model and a spherical grid for solving the equations of the WS model. This results in a set of ordinary differential equations:

$$\frac{dq}{dt} + \underset{\approx}{A}(\mathbf{q}, \mathbf{r}; \tau) = Q_\tau$$

$$\underset{\approx}{B}(\mathbf{q}, \mathbf{r}; \tau) = R_\tau, \tag{27}$$

where $\mathbf{q}$ is an $n$-dimensional vector that contains the salinity and temperature at all grid points, the $m$-dimensional vector $\mathbf{r}$ contains the other model variables, for which no time-derivatives occur: density and the two velocity components. Here, $\underset{\approx}{A}$ and $\underset{\approx}{B}$ are two (nonlinear) operators: $\underset{\approx}{A} : \mathbb{R}^{n+m} \to \mathbb{R}^n$, $\underset{\approx}{B} : \mathbb{R}^{n+m} \to \mathbb{R}^m$. They model, among other things, advection and diffusion of heat, salt, and momentum. The right-hand sides, $Q_\tau$, and, $R_\tau$, are inhomogeneous terms due to surface forcing; $\tau$ represents all model parameters, some of which appear in the surface forcing $Q_\tau$ and $R_\tau$. For a typical experiment with a resolution of $40 \times 20$ grid points $n = 1600$ and $m = 2400$. If at a given parameter setting $\tau_0$ a steady-state solution $(q_0, r_0)$ of the system is known, a new equilibrium can be calculated when one of the parameters, for instance the Rayleigh number or the strength of the salinity flux, is changed by a small amount, $(\tau_0 \to \tau_1)$. Pseudo-arclength continuation is used to calculate the new steady-state solution $(q_1, r_1)$. For a technical introduction to this numerical technique the reader is referred to Seydel (1988). This method enables one to calculate a branch of equilibrium solutions and detect bifurcation points at which the behav-

TABLE 1. Parameter settings.

| Parameter | Value |
|---|---|
| $\delta$ | $10^{-3}$ |
| Pr | 2.25 |
| Ra | $5 \times 10^3$ |
| $E$ | $4 \times 10^{-3}$ |
| $B$ | 50 |
| $r_v$, $r_d$ | 1 |
| $R_S$ | 0.32 |
| $a$ | 0.1 |
| $F_0$ | 6 |

ior and the stability of the system change. To assess the linear stability of the solution $(\mathbf{q}_1, \mathbf{r}_1)$, suppose that we perturb it by infinitesimal perturbations $(\delta\mathbf{q}, \delta\mathbf{r})$. They satisfy the homogeneous equations:

$$\frac{d\delta q}{dt} + \underset{\approx}{A}(\mathbf{q}_1 + \delta\mathbf{q}, \mathbf{r}_1 + \delta\mathbf{r}; \tau_1) = 0$$

$$\underset{\approx}{B}(\mathbf{q}_1 + \delta\mathbf{q}, \mathbf{r}_1 + \delta\mathbf{r}; \tau_1) = 0. \qquad (28)$$

If we assume that the perturbation is of the form $\delta q = \delta\hat{q} \exp(\lambda t)$, and similar for $\delta r$, then the linear stability of the equilibrium solution $(q_1, r_1)$ follows from the linear eigenvalue problem:

$$\lambda\delta\hat{q} + L_{\underset{\approx}{A}}(\delta\hat{q}, \delta\hat{r}) = 0$$

$$L_{\underset{\approx}{B}}(\delta\hat{q}, \delta\hat{r}) = 0, \qquad (29)$$

where $L_{\underset{\approx}{A}}$ and $L_{\underset{\approx}{B}}$ denote the respective linearizations of $\underset{\approx}{A}$ and $\underset{\approx}{B}$ at $(q_1, r_1, \tau_1)$. The structure of the eigenfunction $(\hat{q}, \hat{r})$ at a bifurcation point gives information about what perturbation critically results in a balance between stabilizing and destabilizing effects. For more details on the numerical continuation technique, how to efficiently solve the eigenvalue problem, etc. the reader is referred to Dijkstra et al. (1995), Speich et al. (1996), or Seydel (1988).

## 5. Results

A comparison is made between two 2D models: the Navier–Stokes model and the model by Wright and Stocker. Both models experiments were performed similar to the one described by Quon and Ghil (1992): under mixed surface boundary conditions, the amplitude $\hat{Q}_s$ of the applied salt flux is varied. Although the physical relevance of mixed boundary conditions is questionable, they have nevertheless been used for the purpose of comparison with earlier results. For the same reason, the Rayleigh and Prandtl numbers are given the same value as in the paper by Quon and Ghil (1992): Ra = $5.10^3$, Pr = 2.25. These values result when the following scales, viscosities, and diffusivities are chosen:

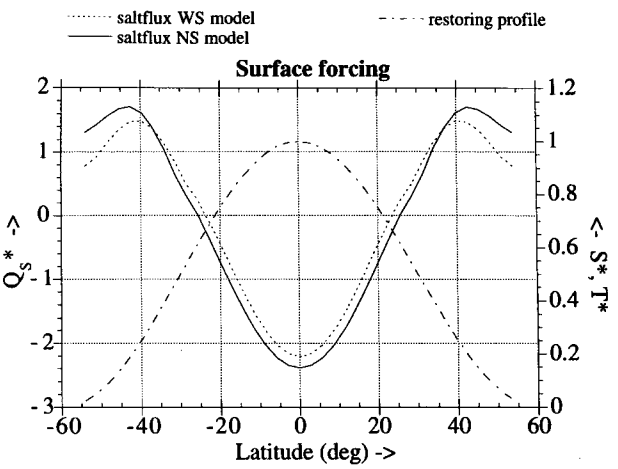


FIG. 1. The surface forcing for both models: the restoring profile for $S^*$ and $T^*$ is shown by the dashed–dotted line (right-hand axis). The salinity fluxes $Q_s^*$, diagnosed from this in the restoring boundary conditions experiment, is shown by the solid (NS model) and the dotted (WS model) lines (left-hand axis).

$$L = 10^6 \text{ m}; \quad D = 10^3 \text{ m}; \quad g = 10 \text{ m s}^{-2};$$

$$\alpha = 10^{-4} \text{ K}^{-1}; \quad \beta = 10^{-4} \text{ (ppm)}^{-1};$$

$$\bar{T} = 25 \text{ K}; \quad \bar{S} = 3.2 \text{ ppm}; \quad \kappa_h = 10^5 \text{ m}^2 \text{ s}^{-1};$$

$$\kappa_v = 10^{-1} \text{ m}^2 \text{ s}^{-1}; \quad A_h = 4.7 \cdot 10^4 \text{ m}^2 \text{ s}^{-1};$$

$$A_v = 4.7 \cdot 10^{-2} \text{ m}^2 \text{ s}^{-1}.$$

The geometrical scales are not precise but roughly those of a schematic ocean. In the WS model the same Prandtl numbers are used, together with $\epsilon_0 = 0.3$. Under identical restoring boundary conditions the WS model was tuned to yield a density distribution corresponding

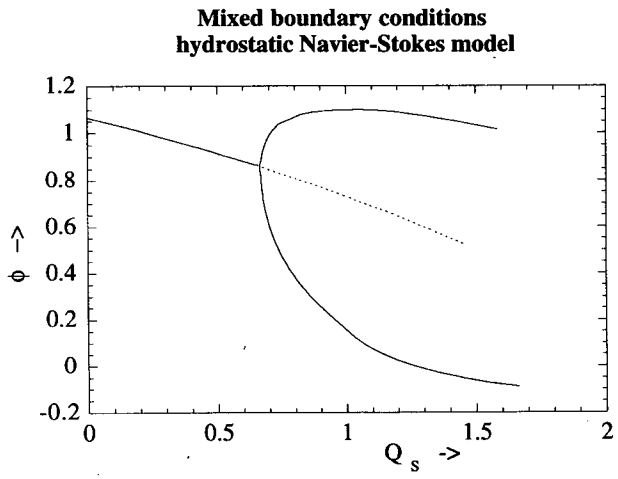


FIG. 2. Bifurcation diagram of the Navier–Stokes model. Plotted along the vertical axis is $\phi$: the value of the streamfunction in a point at middepth at $y = -0.85$. Solid lines indicate linearly stable equilibria; the dotted line linearly unstable equilibria.

to that of the NS model. This suggested $B = 50$, meaning that $E = 4 \times 10^{-3}$. The values of all nondimensional parameters of the model are listed in Table 1.

The salt flux applied to both models was diagnosed from a preliminary experiment. In this experiment, surface salinity and surface temperature were relaxed to the symmetrical idealized profile (Fig. 1):

$$S^*(\theta) = T^*(\theta) = 1/2(1 + \cos 3\theta).$$

The profiles correspond roughly to the observed meridional structure of sea surface temperature and salinity: high at low latitudes and low at high latitudes. The restoring coefficients $\mu_s'$ and $\mu_h'$, see (18) and (19), were set to $10^3$ so that the surface temperature and salinity are essentially fixed ("restoring boundary conditions"). The salt fluxes diagnosed from this solution are symmetrical and are also shown in Fig. 1. Note the similarity between the fluxes of the two models.

### a. *Navier–Stokes model*

The aspect ratio $\delta$ of the large-scale ocean geometry ($\delta = 10^{-3}$) is much smaller than in the original paper by Quon and Ghil (1992) ($\delta = 10^{-1}$). It is this smallness of $\delta$ that motivated the hydrostatic approximation of section (2a). In this zeroth-order equation $\delta$ itself, obviously, does not appear any more. However, its finite magnitude is felt in the parameters $r_v$ and $r_d$ in the transport equations (cf. section 2). If no salt flux is applied, $\hat{Q}_s = 0$, the solution is in a thermal regime and consists of two symmetrical cells with downwelling at high latitudes, where surface density is highest. If the strength of the salt flux is increased from zero, the intensity of the circulation diminishes. The salinity flux has a structure that "introduces" salt through the surface at low latitudes and "removes" salt at high latitudes, thus opposing (and reducing) the density gradient set by the surface temperature. This slows down the flow, shown in the bifurcation diagram for the NS model (Fig. 2). It shows $\phi$, a scalar measure for the complete solution: the value of the streamfunction in a point at mid-depth near the southern boundary. At $\hat{Q}_s = 0.67$ the symmetrical two-cell circulation becomes unstable and two asymmetrical solutions branch off: one with a dominant northern cell, represented by the lower branch, and one with a dominant southern cell, the upper branch. When $\hat{Q}_s$ is increased further, the dominant cell gains in strength, and the small cell disappears completely. Two solutions are shown at $\hat{Q}_s = 1$: the symmetrical one (Fig. 3), which is linearly unstable, and an asymmetrical one (Fig. 4), which is linearly stable. The symmetrical one corresponds with the solution obtained under restoring boundary conditions. This accounts for the identical temperature and salinity distributions in this case, Fig. 3c. Quon and Ghil found similar behavior and similarly looking solutions. Their value for the bifurcation point was different: $\hat{Q}_s = 0.40$. So, the absence of nonhydrostatic

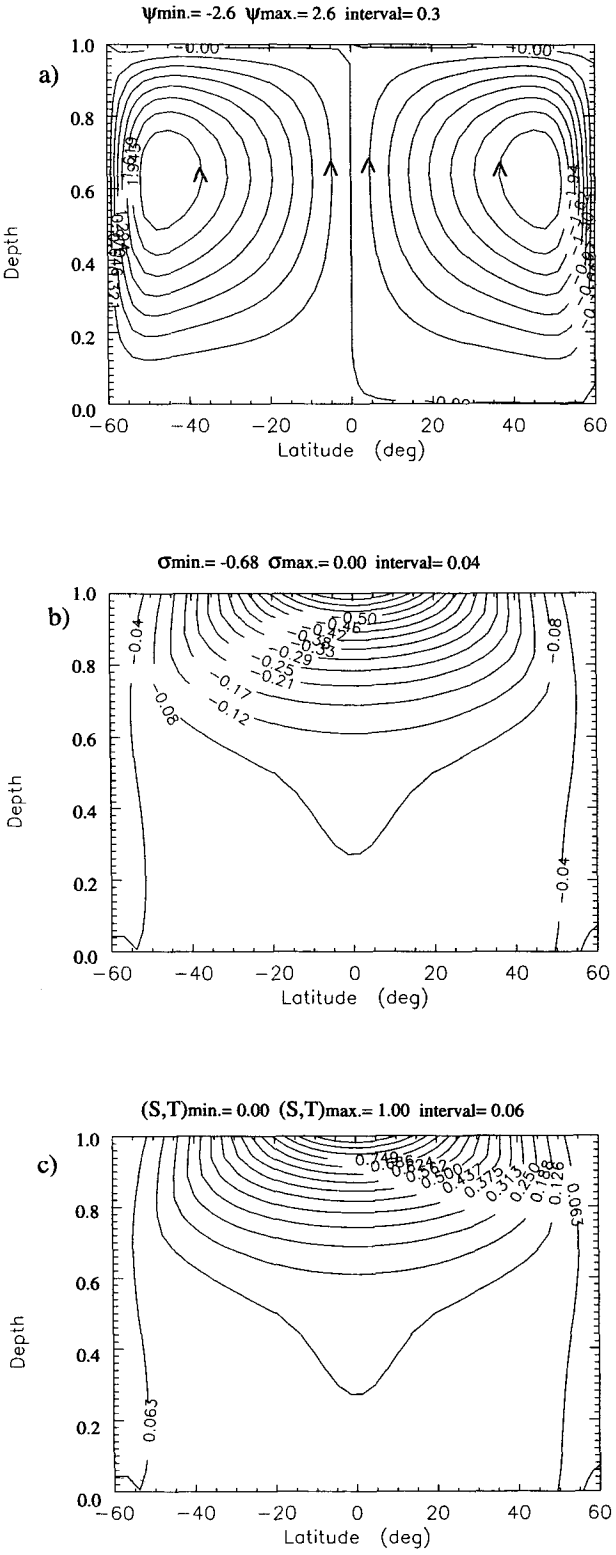


FIG. 3. Symmetrical solution of the Navier–Stokes model at $\hat{Q}_s = 1$ (linearly unstable): (a) streamfunction (the sense of circulation is indicated by arrows), (b) density, and (c) salinity and temperature. For all contour plots the extrema and contour intervals are given at the top of each plot.

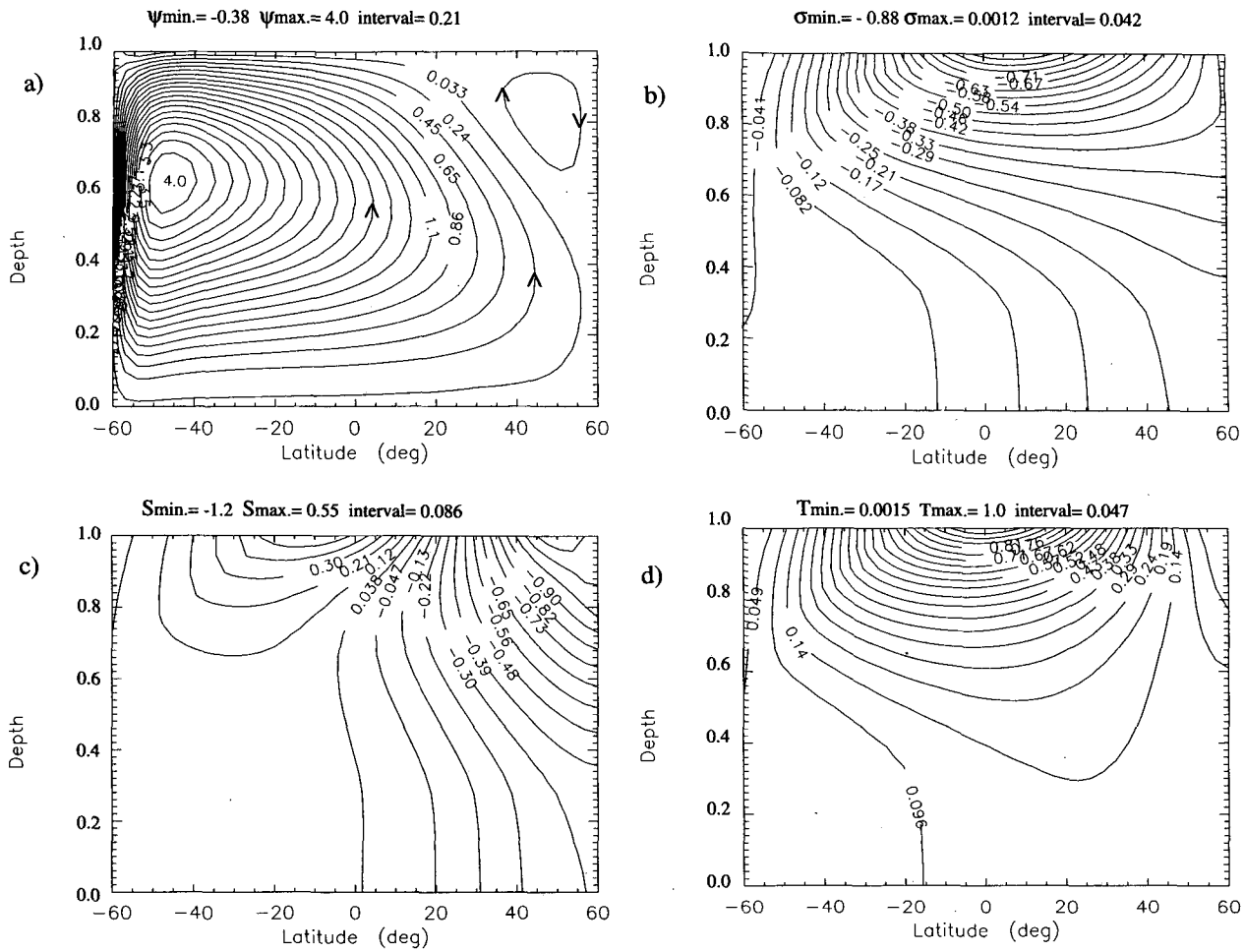


FIG. 4. Asymmetrical solution of the Navier–Stokes model at $\hat{Q}_s = 1$ (linearly stable): (a) streamfunction, (b) density, (c) salinity, and (d) temperature.

effects results in a circulation that is slightly (but not dramatically) more stable. The most unstable eigenfunction (with eigenvalue zero) has been calculated in the bifurcation point (Fig. 5). It will be discussed in the next section, when it is compared with the eigenfunctions of the WS model.

Apparently the process of symmetry breaking is robust to the way in which vertical mixing of buoyancy is described at different aspect ratios: either through accelerations in the vertical momentum equation at a small but finite aspect ratio or through a parameterization based on the IVD scheme in the transport equations in a hydrostatic context.

### *b. Wright and Stocker model*

A comparison between the WS and hydrostatic NS models will bring out whether details of the formulation of the flow dynamics are of great importance to the stability of the flow. Stated differently: does the pitchfork bifurcation survive if the meridional momentum equation (6) is replaced by a zonally averaged variant of the geostrophic balance (25) as discussed in section 3b. The surface salinity flux that has been diagnosed under restoring boundary conditions is shown in Fig. 1 by the dashed line. The same experiment as in the previous section has been carried out for the WS model. The corresponding bifurcation diagram in Fig. 6 features $\phi$ again and indicates that the dynamical behavior of the WS model is quite similar to that of the NS model. If no salt flux is applied, $\hat{Q}_s = 0$, the model is in a thermal mode with two symmetrical circulation cells. It becomes linearly unstable if $\hat{Q}_s$ is increased to 1.07. The basic solution in the bifurcation point is shown in Fig. 7. At that point the symmetrical solution loses its stability, and two asymmetrical solutions branch off in a subcritical pitchfork bifurcation. The general features of the symmetrical and asymmetrical solutions are much like that of the NS model. When the dominant cell has grown to a size that occupies

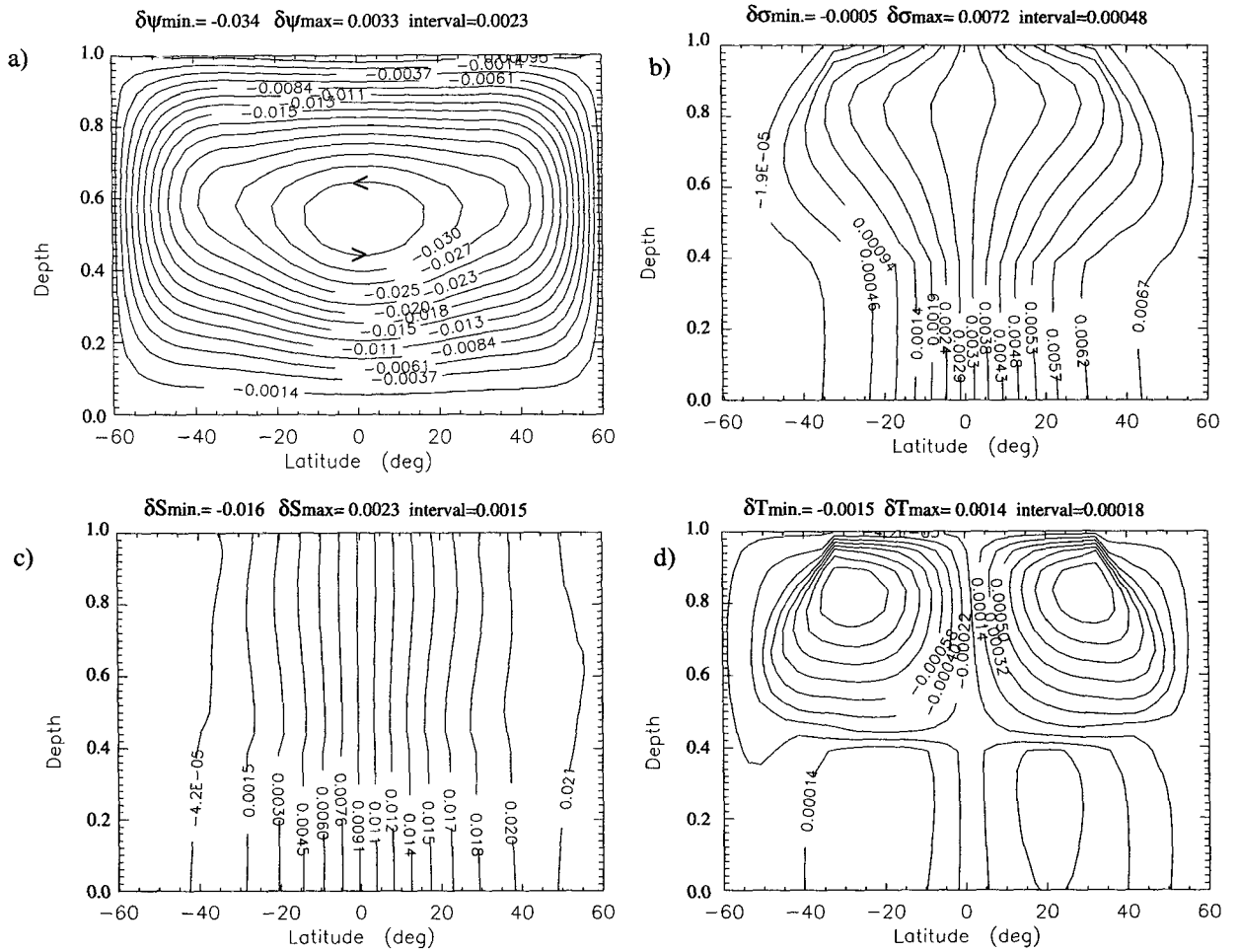


FIG. 5. Most unstable mode of the Navier–Stokes model in the bifurcation point: (a) perturbation streamfunction, (b) perturbation density, (c) perturbation salinity, and (d) perturbation temperature.

nearly all of the basin, a further increase of the salt flux hardly alters the flow near its rising branch. This results in $\phi$ (the streamfunction near the southern wall) showing little dependence on $Q_s$ for the northern sinking solution (the "flat" part of the lower branch of Fig. 6).

The bifurcation structure implies that the WS model at this parameter setting is linearly stable to a switch from restoring to mixed boundary conditions, at $\hat{Q}_s = 1$. That the bifurcation point need not always be situated below $\hat{Q}_s = 1$ is interesting: It means that a switch from restoring to mixed boundary conditions is not necessarily accompanied by loss of linear stability from the (symmetrical) solution. For different forcing, a parameter setting that was less diffusive, and a different convection scheme Wright and Stocker (1991) found the symmetrical solution to be unstable for such a switch. Thus, within the range of modeling uncertainties (values for diffusivities, parameterization of convection, etc.), it is feasible that the bifurcation point can have a value of either more or less than unity. In fact, it was found that, when vertical diffusivity was quadrupled while everything else was unaltered, the system becomes unstable for a switch since bifurcation occurs at $Q_s = 0.9$. The critical location of the bifurcation value can be observed in GCMs as well. The circulation found by Bryan (1986), which he called "essentially equatorially symmetric" after the switch and after a salinity perturbation, suggests a bifurcation slightly below one: under the diagnosed flux ($\hat{Q}_s = 1.$) the system could be driven to one of the stable branches by an asymmetric perturbation. Being so close to the bifurcation point, at $\hat{Q}_s = 1$ the asymmetrical features must have been little developed.

Although the symmetrical solutions of the two models lose their stability for different values of the strength of the salt flux, it is remarkable how robust this pitchfork bifurcation appears to be: with two 2D models that have completely different momentum budgets the same qualitative behavior is found under mixed boundary

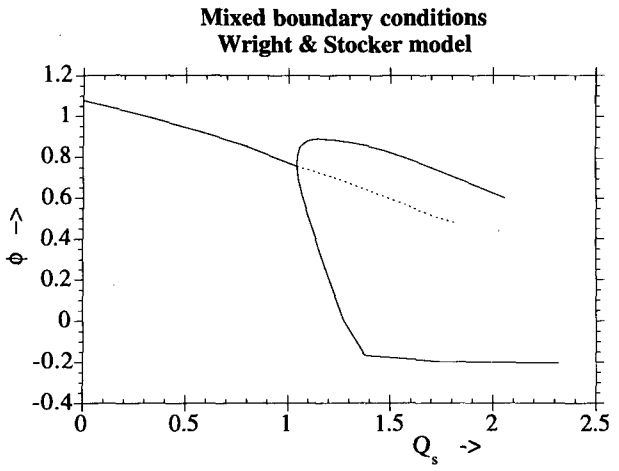


FIG. 6. Bifurcation diagram of Wright and Stocker model. Plotted along the vertical axis is $\phi$: the value of the streamfunction in a point at middepth at $\theta = 54°$S. Solid lines indicate linearly stable; the dotted line linearly unstable equilibria.

conditions. The qualitatively similar behavior, however, suggests that the essentials of symmetry breaking of the thermally dominated circulation are not in the dynamics, but can be deduced from the transport equations for heat and salt. This is in agreement with the results of a study by Thual and McWilliams (1992), in which advection of momentum was neglected altogether but still a transition from symmetrical to asymmetrical solutions was found. In the next section an analysis of the linear instability of the symmetrical circulation will be presented.

## 6. Linear stability analysis

For both models the eigenfunctions that correspond with the zero eigenvalue at the bifurcation were calculated. These eigenfunctions consist of all five simulated fields, that is, temperature, salinity, density, and the two velocity components (Figs. 5 and 8). Since the basic solutions satisfy the boundary conditions of sections 2b and 3b respectively, the eigenfunctions have to satisfy the corresponding homogeneous boundary conditions. In particular, the temperature eigenfunction and the salinity flux must be zero at the surface. Since all boundary conditions for the salinity eigenfunction are of flux type, it is not uniquely determined. As with the basic solution, one salinity field is selected that is zero in a certain grid point. The eigenfunctions are determined up to a multiplicative constant, as can be seen from (29). Of course, the ratio of the five components is fixed.

As was the case for the basic solutions, there is again a strong qualitative similarity between the eigenfunctions of both models. This essentially means that beyond the respective bifurcation point, the basic solution of each model can be destabilized by infinitesimal perturbations with similar spatial structures. An infinitesimal perturbation to the basic solution in the bifurcation point of for instance the WS model, which has the structure of the eigenfunction of Fig. 8, will remain stationary. Its interaction with the basic solution results in a critical balance between stabilizing and destabilizing processes: the perturbation neither grows nor decays. By looking at this interaction in some detail one can learn about the cause of the symmetry breaking that occurs if the perturbation were added at a slightly higher value of $\hat{Q}_s$.

Suppose that we add to the basic solution (indicated by subscripts 0) a salinity perturbation $\delta S$ that has the shape of the salinity eigenfunction (Fig. 8c): that is, it is nearly vertically homogeneous and has a monotonic meridional gradient, weakening toward the high latitudes. Forgetting for the moment about temperature effects, this salinity perturbation gives rise to a density gradient that causes a velocity perturbation $\delta\mathbf{u} = (\delta v, \delta w)$ with roughly the shape of the one-cell circulation of Fig. 8a. The two perturbation fields interact with the basic solution to determine the time evolution of $\delta S$ (quadratic perturbation terms are neglected):

$$\frac{\partial \delta S}{\partial t} = -\left( \nabla \cdot \underbrace{(\delta S \mathbf{u}_0)}_{\text{direct}} + \nabla \cdot \underbrace{(S_0 \delta \mathbf{u})}_{\text{indirect}} - \mathrm{Pr}^{1/2} \nabla^2 \delta S \right).$$

Diffusion will attempt to destroy the perturbation, so it is particularly the two advective fields that interest us here: this interaction of perturbation and basic solution can enhance or impede the growth of the perturbation. The first advective term represents the direct advection of the perturbation by the basic solution (direct salt feedback). Its meridional component is shown in Fig. 9a. The second advective term (indirect salt feedback) describes the advection of the basic salinity field by the velocity perturbation. Its meridional component is shown in Fig. 9b. The vertical components of both fluxes are either small themselves, or yield little contribution to the divergence, when compared to the meridional components, and are not shown. Regions where the divergence of either flux is positive are indicated by dark shading. Those regions where the divergence is negative are marked by a light shade. Regions with negligible divergence in the transport are white.

Over much of the "Northern Hemisphere's" surface layer the direct salinity feedback will reduce $\delta S$. Consequently, the meridional gradient of the salinity perturbation, its main feature, will decrease here. The direct feedback is thus found to have a stabilizing effect. Due to the symmetry of both basic salinity $S_0$ and the velocity perturbation $\delta\mathbf{u}$, the indirect salinity feedback is symmetrical around the equator. The divergence of this field, however, is antisymmetrical and enhances this gradient by increasing (decreasing) the salinity perturbation over the whole Northern (Southern)

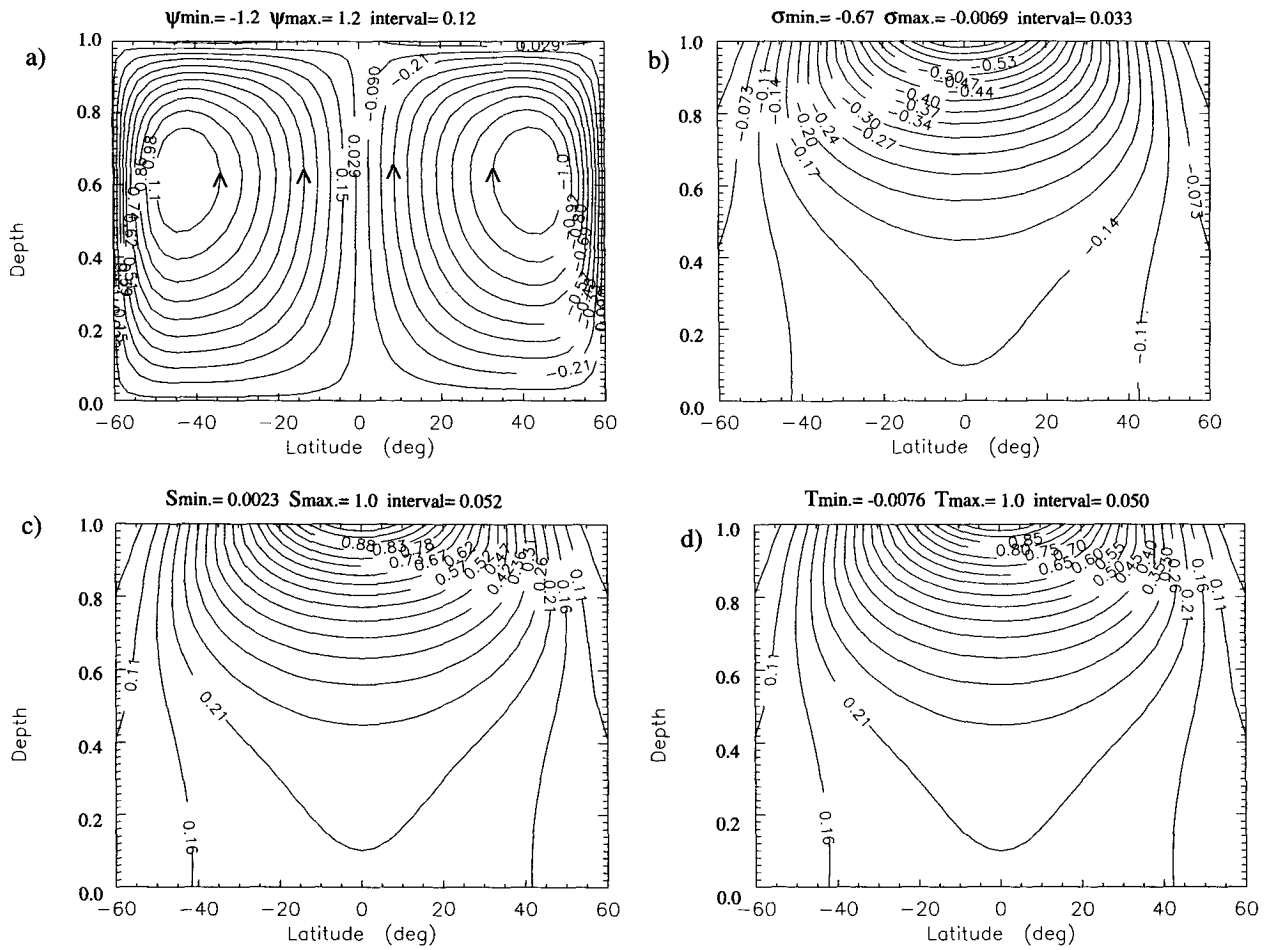


FIG. 7. Basic solution of the Wright and Stocker model at $\hat{Q}_s = 1.07$: (a) streamfunction, (b) density, (c) salinity, and (d) temperature.

Hemisphere. The indirect salinity feedback thus has a destabilizing effect. At this parameter setting these two fluxes, together with the diffusive fluxes (that have not been discussed), are critically at balance. A loss of stability can be expected if the indirect advective flux were to gain in strength. It is important to remember that during this interaction no salt is "lost" or "gained" from the atmosphere, due to the no-flux condition.

Now we turn to the temperature perturbation. The velocity perturbation interacts with the basic temperature $T_0$ to give a meridional heat transport $\delta v T_0$ (Fig. 9c) that closely resembles the "indirect salinity transport" $\delta v S_0$. The corresponding vertical flux $\delta w T_0$ is again an order of magnitude smaller and hardly contributes to the divergence. This divergence gives rise to a temperature perturbation $\delta T$ (Fig. 8d) that has a quadrupole-like structure that is markedly different from the salinity perturbation (Fig. 8c). Although the transport equations for both fields are exactly the same, the surface boundary conditions are different: zero perturbation salinity flux versus a zero perturbation temperature. The latter condition inhibits the isotherms from having a vertical intersection with the surface, like they have at the bottom (no perturbation heat flux through the bottom). The isohalines of $\delta S$, on the other hand, intersect surface and bottom vertically. Note also that the amplitude of the temperature perturbation is two orders of magnitude smaller than the salinity perturbation. The buoyancy ratio density $R_S$ (section 2a) is set to 0.32 in this experiment. Because of this, the effect of the perturbation temperature is enhanced and the isopycnals do not run parallel to the isohalines. However, the overall structure of the density as implied by salinity remains, and only details of the velocity field are changed by the temperature.

Now one may wonder what the role of temperature is then in the whole process of symmetry breaking. First, remember that the direct salinity feedback acts in a stabilizing way. To reduce its influence the basic velocity $\mathbf{u}_0$ should be decreased. Since the flow is in a thermally dominated regime, it is the reduced role of temperature that makes that an increase of the salinity

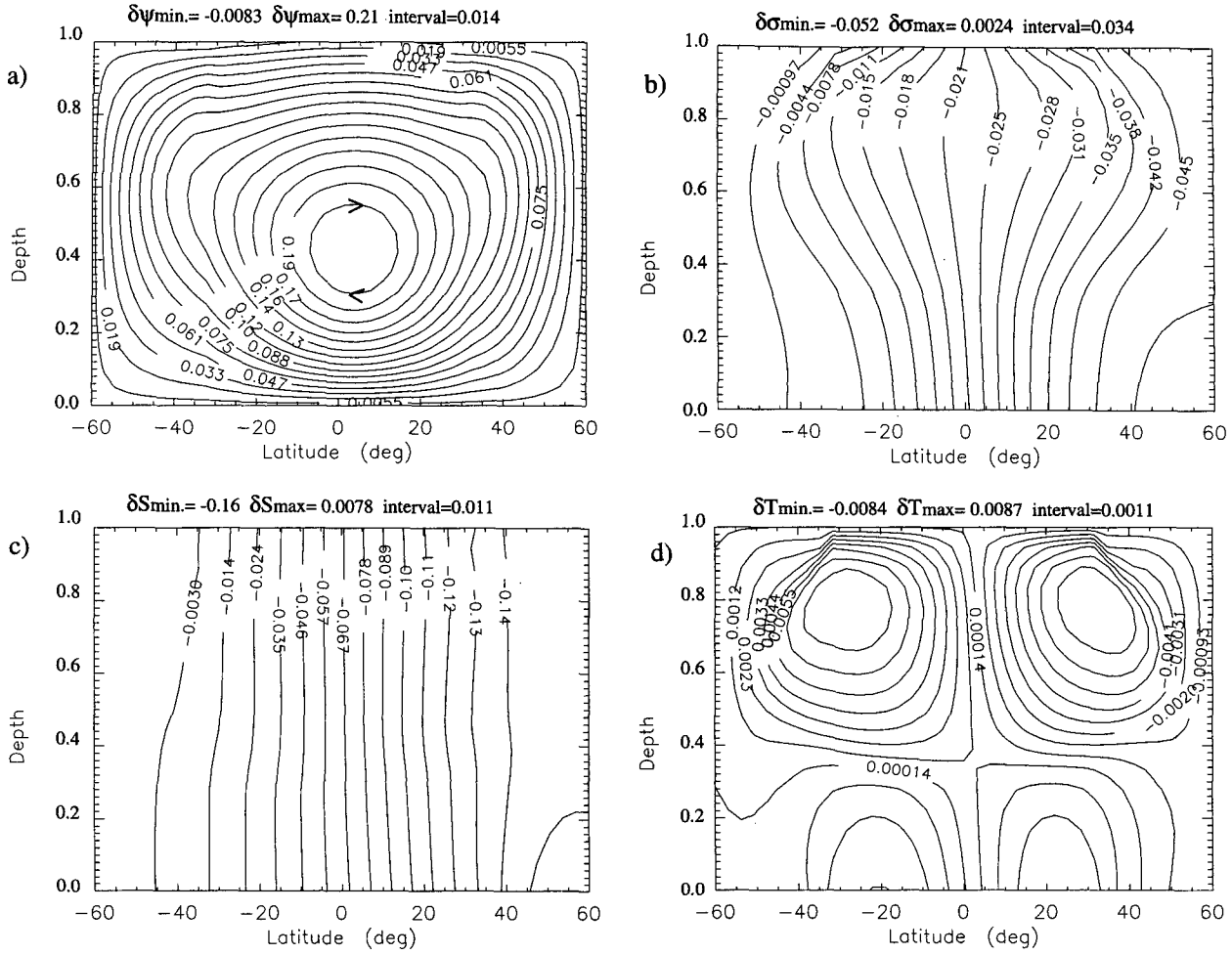


FIG. 8. Most unstable mode of the Wright and Stocker model in the bifurcation point: (a) perturbation streamfunction, (b) perturbation density, (c) perturbation salinity, (d) perturbation temperature.

flux results in a smaller basic velocity other than just increasing basic salinity. These two factors combine to shift the balance between the direct and indirect advective salinity fluxes suggested above. In a point on the symmetrical branch beyond the bifurcation (linearly unstable solution), this is exactly what is found (see Fig. 10). This figure shows the same interaction fields at $\hat{Q}_s = 1.2$.

That the salinity eigenfunction has a nearly vertically homogeneous structure supports the view that the onset for the loss of stability is not the modification of the surface salinity, and a resulting shutdown of convection. Rather, this instability is triggered by an advective process as described above. It is consistent with reasoning by, for instance, Marotzke et al. (1988).

With this mechanism, the factors that determine the value for the bifurcation point can be understood. Given a certain basic solution to which an infinitesimal salinity perturbation is added. The velocity perturbation that results from this should be strong enough to overcome the stabilizing effect of the direct feedback to bring about a loss of symmetry.

Can we then understand why the NS model can be destabilized at a lower value of the salinity flux than can the WS model? If we look in more detail to the velocity eigenfunctions, we see that in the NS model the perturbation streamfunction possesses reflection symmetry with respect to the lines $z = 1/2$ and $y = 0$ (Fig. 5a). Stated differently, the center of circulation of the velocity eigenfunction lies in the center of the basin. In the WS model, this eigenfunction has no symmetry of reflection around the line $z = 1/2$. The center of circulation is shifted downward to approximately $z = 0.4$ (Fig. 8). To guarantee a vanishing northward mass flux, the meridional velocity in the upper part is smaller than in the lower part. For the destabilizing role of the indirect salinity advection this means that the northward advection of salt in the upper half is comparatively weakened. So, for a given density pertur-

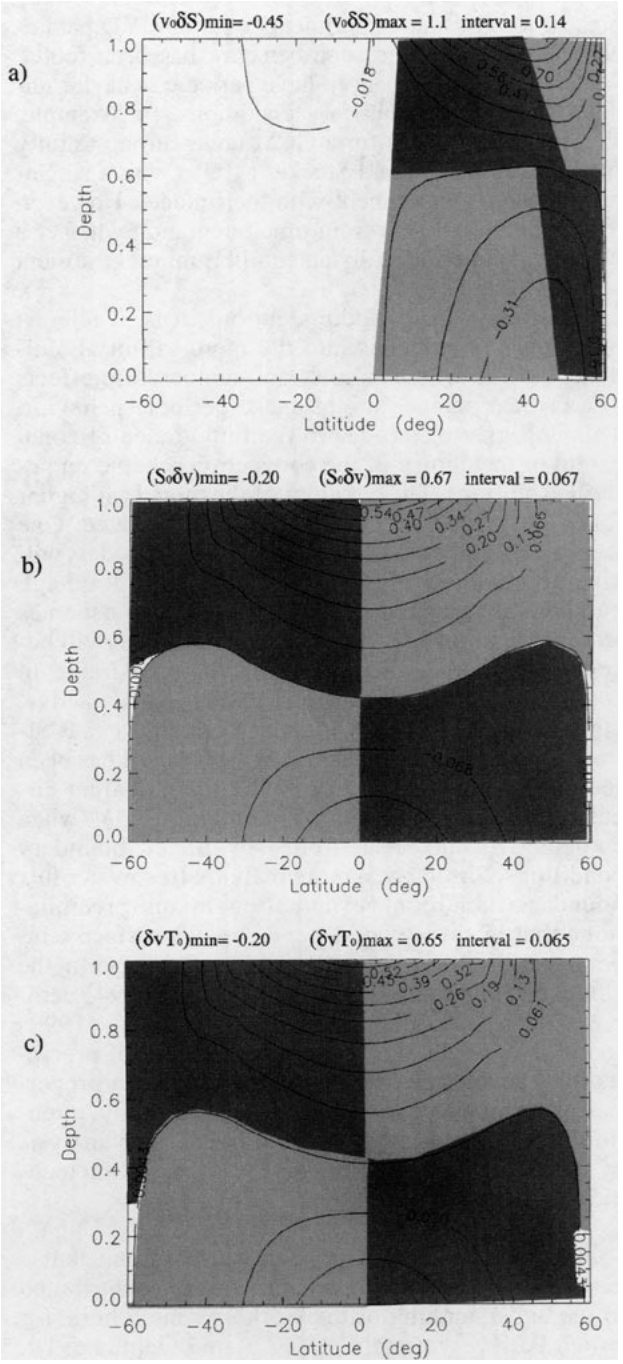


FIG. 9. Interaction fields of basic solution and perturbation of the WS model in the bifurcation point ($\hat{Q}_s$ = 1.07). (a) Direct salinity feedback ($v_0\delta S$), (b) indirect salinity feedback ($S_0\delta v$), (c) indirect temperature feedback ($\delta v T_0$). Dark (light) shading indicates positive (negative) divergence of the respective flux; white means weak divergence.

bation, the WS model generates a less effective indirect salinity feedback than the NS model, so that the latter can be destabilized for a lower value of the salt flux, or a stronger circulation of the basic solution.

## 7. Conclusions

I have used two different models of a two-dimensional thermohaline flow to study the impact of an increased salt flux on a state that is thermally dominated. The two models differ only in their momentum budget: one model essentially represents a nonrotating (vertical) sheet of water with a very small aspect ratio. The other model accounts for the Coriolis torque that acts on the meridional plane when the system is subjected to rotation. The two models further have the same features, for example, the transport equations for heat and salt and the implicit vertical diffusion scheme, which removes static instability (convective adjustment). To assess the influence of nonhydrostatic effects and aspect ratio one can compare the current results with those of Quon and Ghil (1992).

With similar parameter settings the two models of the present study were subjected to the same experiment: under mixed boundary conditions, the strength of the applied salt flux was increased from zero onward. This experiment gives, in a systematic way, insight into the behavior of the system when moving from a thermal to a more haline but still thermally dominated regime. The thermal solution consists originally of two symmetrical cells but becomes unstable at some critical strength of the salt flux, and two new branches of asymmetrical solutions emerge. Although the points of bifurcation differ in the two models, in a qualitative sense they are identical. This is reflected in the structure of the most unstable eigenfunction at the respective bifurcation points. When the current experiments with the NS model and those described by Quon and Ghil (1992) are compared, it appears that the loss of symmetry of the thermal circulation is affected only in a quantitative way by nonhydrostatic effects at a larger aspect ratio. This correspondence in the dynamical behavior of different models confirms the idea that, at least in the thermal regime, the loss of symmetry is very insensitive to the details of the momentum budget (such as the presence of rotation) and can be understood by examining the transport equations for heat and salt. It also explains why the phenomenon of multiple equilibria occurs in such a wide range of models—Stommel's (1961) box model, the different two-dimensional models (Marotzke et al. 1988; Wright and Stocker 1991; Quon and Ghil 1992) and GCMs (Bryan 1986; Weaver et al. 1993)—as long as some advection mechanism is present. Symmetry breaking does not depend critically on the particular convection scheme that is used.

In none of the experiments have we encountered any periodic solutions. This obviously means that in this part of parameter space a sustained oscillation is not an equilibrium state of the system, neither stable nor unstable. It has been observed that the spinup run for a model under restoring surface boundary conditions ends in a "quasi steady" state, where intermittent con-

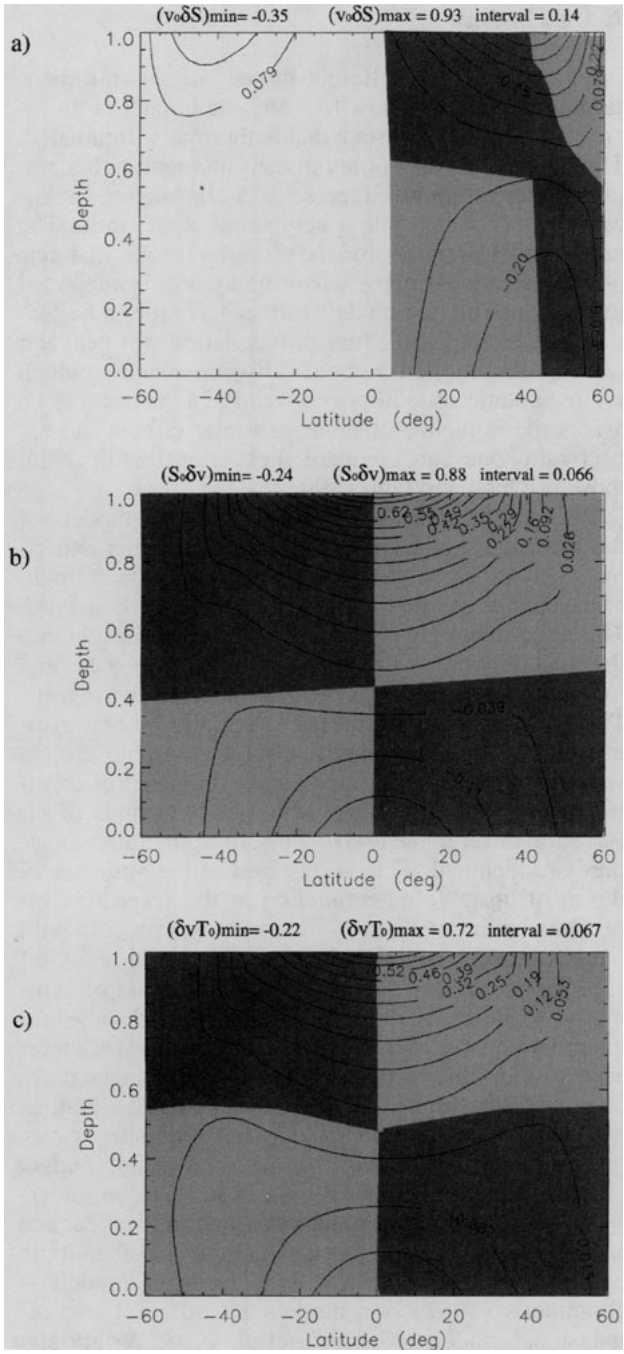


FIG. 10. Interaction fields of basic solution and perturbation of the WS model outside the bifurcation point ($\hat{Q}_s = 1.2$. (a) Direct salinity feedback ($v_0\delta S$), (b) indirect salinity feedback ($S_0\delta v$), (c) indirect temperature feedback ($\delta v T_0$). Dark (light) shading indicates positive (negative) divergence of the respective flux; white means weak divergence.

vection causes small oscillations (e.g., see Bryan 1986; Hovine and Fichefet 1994). Marotzke (1991) argued that an (oscillating) numerical mode can be excited with the "standard GFDL convection scheme." In the present steady-state experiments with the IVD parameterization scheme no such behavior has been found. Different models appear to have periodic behavior under steady mixed boundary conditions, for example, Weaver et al. (1993) for a GCM under strong salinity forcing and Wright and Stocker (1991) with a single-hemispherical experiment with their model. However, it is difficult to assess from time integration whether a periodic solution is really an equilibrium or a transient solution of the system.

With regard to periodic solutions, it is of interest to follow the branches into the more salinity-dominated regime where salinity and temperature effects at a critical balance might cause periodic behavior. This will give us an idea to the importance of zonal extent or the choice of the convection scheme on periodic solutions. The behavior of the models at higher Rayleigh numbers will have to be investigated. One would expect that the behavior of the two models will diverge qualitatively for an increasing Rayleigh number. At a given density field, advection becomes stronger, and differences in the velocity field will become more pronounced. Finally, it is desirable to couple the ocean to a more realistic, that is, active, atmosphere. A surface boundary condition that allows for variable atmospheric heat transport has been found to increase stability of the thermohaline circulation (Rahmstorf and Willebrand 1995), when compared to an ocean forced by mixed boundary conditions. Similarly, a more realistic freshwater flux boundary condition (evaporation minus precipitation) that in some way depends on sea surface temperature has been shown to affect stability. In the context of box models, Nakamura et al. (1994) demonstrated a destabilizing effect. Stocker et al. (1992) found that details of the parameterization of precipitation can strongly determine the attraction properties of a global ocean model. In a future study, attention will be given to both these issues. For analysis of such simple coupled models the continuation technique provides a useful tool.

*Acknowledgments.* The many discussions that I had with Dr. C. B. Vreugdenhil greatly contributed to the understanding of the work presented here, for which I am very grateful. Also, I am indebted to Dr. H. A. Dijkstra and M. J. Molemaker, who provided the numerical continuation code and made me familiar with it when I applied it to thermohaline models. Two anonymous reviewers are appreciated for their useful remarks and suggestions. This work was made possible through Grant 770 03 234 of the Netherlands' Organization for Scientific Research (NWO). Part of the computations were performed on the CRAY Y-MP at the Academic Computer Centre (SARA), Amsterdam, The Netherlands, and sponsored by the National Computing Facilities (NCF).

## REFERENCES


Arakawa, A., and V. Lamb, 1977: Computational design of the basic dynamical processes of the UCLA general circulation model. *Methods Comput. Phys.*, **17,** 173–265.

Bryan, F., 1986: High-latitude salinity effects and interhemispheric thermohaline circulations. *Nature,* **323,** 301–304.

Dijkstra, H., M. J. Molemaker, A. van der Ploeg, and E. F. F. Botta, 1995: An efficient code to compute non-parallel steady flows and their linear stability. *Comput. Fluids,* **24,** 415–434.

Harvey, L. D. D., 1992: A two-dimensional ocean model for long-term climatic simulations: Stability and coupling to atmospheric and sea-ice models. *J. Geophys. Res.*, **97**(C6), 9435–9453.

Hovine, S., and T. Fichefet, 1994: A zonally averaged, three-basin ocean circulation model for climate studies. *Climate Dyn.,* **10,** 313–331.

Marotzke, J., 1991: Influence of convective adjustment on the stability of the thermohaline circulation of the ocean. *J. Phys. Oceanogr.,* **21,** 901–907.

——, P. Welander, and J. Willebrand, 1988: Instability and multiple steady states in a meridional plane model of the thermohaline circulation. *Tellus,* **40A,** 162–172.

Nakamura, M., P. H. Stone, and J. Marotzke, 1994: Destabilization of the thermohaline circulation by atmospheric eddy transport. *J. Climate,* **7,** 1870–1882.

Pedlosky, J., 1987: *Geophysical Fluid Dynamics.* Springer-Verlag, 710 pp.

Quon, C., and M. Ghil, 1992: Multiple equilibria in thermosolutal convection due to salt-flux boundary conditions. *J. Fluid Mech.,* **245,** 449–483.

Rahmstorf, S., and J. Willebrand, 1995: The role of temperature feedback in stabilising the thermohaline circulation. *J. Phys. Oceanogr.,* **25,** 787–805.

Seydel, R., 1988: *From Equilibrium to Chaos— Practical Bifurcation and Stability Analysis.* Elsevier Science, 367 pp.

Speich, S., H. Dijkstra, and M. Ghil, 1996: Successive bifurcations in a shallow-water model applied to the wind-driven ocean circulation. *Nonlin. Proc. Geophys.,* in press.

Stocker, T., D. G. Wright, and L. A. Mysak, 1992: A zonally averaged coupled ocean-atmosphere model for paleoclimatic studies. *J. Climate,* **5,** 773–797.

Stommel, H., 1961: Thermohaline convection with two stable regimes of flow. *Tellus,* **13,** 224–230.

Thual, O., and J. C. McWilliams, 1992: The catastrophe structure of thermohaline convection in a two-dimensional fluid model and a comparison with low-order box models. *J. Geophys. Astrophys. Fluid Dyn.,* **64,** 67–95.

Wang, H., and G. E. Birchfield, 1992: An energy-salinity balance climate model: Water vapor transport as a cause of changes in the global thermohaline circulation. *J. Geophys. Res.,* **97**(C2), 2335–2346.

Weaver, A. J., and T. M. C. Hughes, 1992: Stability and variability of the thermohaline circulation and its link to climate. *Trends in Physical Oceanography,* Research Trends Series, Council of Scientific Research Integration, 56 pp.

——, J. Marotzke, P. F. Cummins, and E. S. Sarachik, 1993: Stability and variability of the thermohaline circulation. *J. Phys. Oceanogr.,* **23,** 39–60.

Welander, P., 1986: Thermohaline effects in the ocean circulation and related simple models. *Large-scale Transport Processes in Oceans and Atmospheres,* J. Willebrand and D. L. T. Anderson, Eds., Reidel, 163–200.

Wright, D. G., and T. F. Stocker, 1991: A zonally averaged model for the thermohaline circulation. Part I: Model development and flow dynamics. *J. Phys. Oceanogr.,* **21,** 1713–1724.

——, and ——, 1992: Sensitivities of a zonally averaged global ocean circulation model. *J. Geophys. Res.,* **97**(C8), 12 707–12 730.

——, C. B. Vreugdenhil, and T. M. C. Hughes, 1995: Vorticity dynamics and zonally averaged ocean circulation models. *J. Phys. Oceanogr.,* **25,** 2141–2154.